PAPER

Vis-NIR photodetector with microsecond response enabled by 2D bismuth/Si(111) heterojunction

2D Materials

PAPER

RECEIVED
28 November 2020

REVISED
5 February 2021

ACCEPTED FOR PUBLICATION
26 February 2021

PUBLISHED
19 March 2021

Vis-NIR photodetector with microsecond response enabled by 2D bismuth/Si(111) heterojunction

Zhaoying Dang[1,3,5], Wenhui Wang[2,3,5], Jiayi Chen[1], Emily S Walker[4], Seth R Bank[4], Deji Akinwande[4], Zhenhua Ni[2,3,*] and Li Tao[1,3,*]

[1] School of Materials Science and Engineering, Southeast University, Nanjing 211189, People's Republic of China
[2] School of Physics, Southeast University, Nanjing 211189, People's Republic of China
[3] Center for 2D Materials, Southeast University, Nanjing 211189, People's Republic of China
[4] Microelectronics and Engineering Research Center, Department of Electrical and Computer Engineering, The University of Texas at Austin, Austin, TX 78758, United States of America
[5] These authors contribute equally to this work.
[*] Author to whom any correspondence should be addressed.

E-mail: tao@seu.edu.cn and zhni@seu.edu.cn

Keywords: bismuthene, heterojunction, photodetector, optoelectronics, Xene

Supplementary material for this article is available online

Abstract

Atomic sheets of bismuth (Bi) have been expected to yield exotic optoelectronic properties, holding great promise for photodetector devices. However, existing Bi thin film photodetectors have limited performance in terms of photoresponsivity or response time, hindering its practical application. Herein, we report an experimental research progress on optoelectronic properties of epitaxial 2D Bi grown on Si(111) substrate. Our 2D Bi/Si(111) heterolayer exhibits inspiring photodetection performance, including a Vis-NIR broadband response with a responsivity up to 80 A W^{-1} and response time ~3 μs, which is attributed to promoted generation and transportation of charge carriers in the heterojunction. 2D Bi/Si(111) here also demonstrates stable and reproducible photo switching behavior. This work paves an avenue to develop photodetectors based on heterointerface between group VA Xene and Si(111) with rapid switching behavior and adequate photoresponsivity.

1. Introduction

2D mono-elemental materials (Xene), such as phosphorene, have attracted considerable attention because of exceptionally electrical and optical properties [1–3] beyond graphene and transition-metal dichalcogenides. As a cousin of phosphorene, 2D Bi has emerged as a new family member of Xene for microelectronic and optoelectronic applications. Intensive research on systematic magneto transport has proved that ultrathin bismuth (Bi) film is internally insulating but possesses highly conductive surfaces, suggesting that the conductive surface channel is important for carrier transport [4, 5]. The calculated carrier mobility of monolayer Bi is around 1000 cm^2 V^{-1} s^{-1} under room-temperature, indicating far-reaching application in logic transistors [6]. In addition, 2D Bi possesses relatively small indirect bandgap and an optically active bulk layer that crucial for the absorption of light [7]. In light of aforementioned properties, the rational utilization of 2D Bi in device is able to foster carrier transport and modulate bandgaps, making versatile devices available.

Recently, there have been increasing numbers of reports revolving optoelectronic property of Bi nanomaterials. The photo-electrochemical (PEC) performance demonstrated that 4–15 nm Bi nanosheet may possess a great potential as PEC-type photodetector with 1.8 μA W^{-1} responsivity [8]. Approximate 13 nm Bi film photodetector fabricated on flexible polyimide substrate exhibited fast rise time ~30 ms and decay time ~14 ms and reproducibility after bending many times [9]. Moreover, more than 50 nm Bi film photodetector presented 250 mA W^{-1} responsivity and broadband detection range [7]. Current photodetectors based on Bi thin film lack potential applications such as highly sensitive or ultrafast detection.

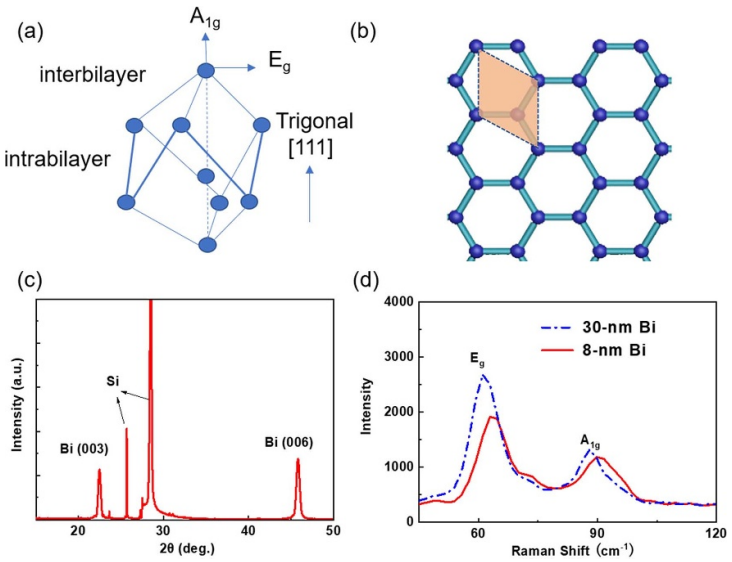

Figure 1. Atomic structure and phase characterization of 2D Bi. (a) Structure of bismuth rhombohedral under side view. (b) Crystal structure of bismuth atoms under top view. (c) XRD pattern and (d) Raman spectra of 2D Bi.

To further improve the optoelectronic performance of Bi thin layer, it is promising to form the heterojunction with semiconductors. For instance, Bi (47 nm)/WS_2/Si photodetector achieved 0.3 A W^{-1} photoresponsivity under 2 V voltage bias [10]. Although ultrathin films of Bi on Si(111) substrate is available via molecular beam epitaxy (MBE) [11], there is still a lack of experimental investigation on photo response of epitaxial 2D Bi/Si(111) heterojunction until now.

Herein, we have carried out a comprehensive study and revealed a dramatic enhancement on optoelectronic properties of epitaxial 2D Bi on Si(111) substrates [12]. The resultant 2D Bi/Si(111) heterojunction device is sensitive to a wide range illumination from visible to near-infrared with high responsivity and fast response speed than single Bi thin film alone. These findings could inspire intensive studies of optoelectronic effects for other similar Xenes.

2. Results and discussion

Bi with rhombohedral crystal structure is formed by stacking of (111)-oriented atomic sheets (figure 1(a)) in hexagonal arrangement (figure 1(b)) [13]. X-ray diffraction (XRD) peaks in figure 1(c) agree well with reported lattice-parameter values (JCPDS 44-1246), and consistent with rhombohedral structure lattice parameters ($a = b = 4.55 \pm 0.01$ Å, $c = 11.86 \pm 0.01$ Å, $\alpha = \beta = 90°$ and $\gamma = 120°$). Moreover, it exhibits single-crystalline structure with preferred orientation (00l) parallel to the film surface [14]. Raman spectra (figure 1(d)) shows two characteristic peaks: ~62 cm^{-1} for E_g and ~91 cm^{-1} for A_{1g} mode that are in conformity with former literature reports [13]. A_{1g} and E_g phonon modes, relevant to the thickness of 2D Bi, are parallel and perpendicular to the trigonal axis respectively. A blue shift of two peaks will occur once it towards to bulk Bi (figure S1 (available online at stacks.iop.org/2DM/8/035002/mmedia)) that can be preliminarily attributed to phonon confinement in 2D Bi [15]. XRD and Raman characterizations both confirm a successful growth of 2D Bi on Si(111) with highly crystalline nature.

It exhibits a uniform and smooth surface for 2D Bi on Si(111) in this study. Energy-dispersive x-ray spectroscopy (EDXs) reveals a uniform distribution of Bi element without any detectable oxidation peak (figure 2(a)). Atomic force microscope (AFM) has observed a smooth surface with root-mean-square roughness ~0.8 nm (figure 2(b)) on our 2D Bi samples. A typical metal–semiconductor–metal photodetector configuration is depicted in figure 2(c) and detailed device fabrication process is shown in section 3. The linear $I_d - V_d$ curve (figure 2(d)) indicates an Ohmic contact between Bi and Ti/Au electrodes. The sheet resistance can be calculated by $R_s = (R \cdot w)/L$, where L is the length of photodetector channel at 5 μm, w is the channel width at 3 μm, and R is the resistance. The obtained sheet resistance is 75 and 104 kΩ sq^{-1} for 8 nm and 30 nm 2D Bi respectively. Higher electrical conductivity in thinner 2D Bi can be ascribed to the increase of surface state induced photocurrent generation as thickness decreases [16].

Electrical property of 2D Bi is further investigated by Hall effect measurement (table 1). Carrier mobility and concentration for 8 nm (or 30 nm) epitaxial 2D Bi on Si(111) are 328 cm^2 V^{-1} s^{-1} (or 254 cm^2 V^{-1} s^{-1}) and 1.69 × 10^{17} cm^{-3} (or 8.26 × 10^{16} cm^{-3}) respectively, higher than counterparts made from pulsed laser deposition and other methods [17, 18]. Furthermore, 8 nm 2D Bi possesses larger carrier concentration (an increase of 104%)

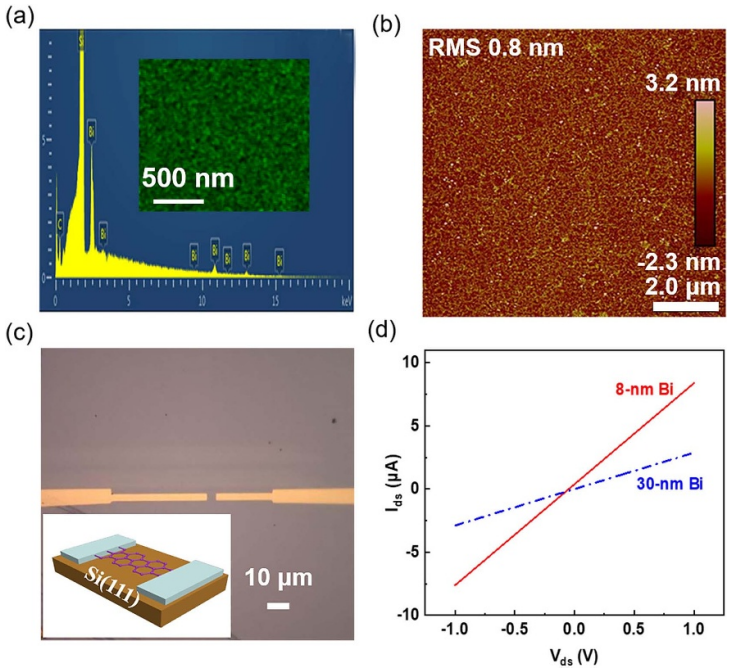

Figure 2. Surface and electrical characterization on 2D Bi/Si(111). (a) AFM and (b) SEM-EDXs images of 2D Bi. Inset: elemental mapping of 2D Bi surface. (c) Optical image of fabricated device with designed Au electrodes. Inset: schematic illustration of heterojunction device layout. (d) Linear output characteristic curve of 8 nm and 30 nm Bi.

Table 1. Hall measurements on 2D and bulk Bi.

Bismuth thickness	Carrier mobility ($cm^2\ V^{-1}\ s^{-1}$)	Carrier concentration (cm^{-3})	Electrical conductivity ($S\ m^{-1}$)
8 nm	328	1.69×10^{17}	894.9
30 nm	254	8.26×10^{16}	335.6
Bulk	3690	8.7×10^{18}	5.1×10^{5}

and higher mobility than 30 nm sample. We propose that as thickness increases to 30 nm, the surface to volume ratio reduces accompanied with a diminishing metallic surface effect, thus leading to a recession on electrical conductivity. However, when further increasing thickness to bulk form, both carrier concentration and charge mobility increase due to the absence of band gap and negligible scattering effect [19].

The photoresponse properties of fabricated 2D Bi/Si(111) photodetector (figure 3(a)) were investigated by photodetection station at room temperature (see section 3 for measurement setup details). Under 532 nm illumination, photocurrent mapping image (figure 3(b)) demonstrates distinct photocurrent stemmed around 2D Bi region between two metal electrodes. The photocurrent generated from 2D Bi/Si(111) heterojunction is much higher than bare Si(111) (figures 3(c) and (d)) plus 2D Bi (figures S2 and S3). Aforementioned performance of the 2D Bi/Si(111) heterojunction photodetector can be ascribed to the following few aspects: (a) enhanced photon absorption to promote photogenerated charge carriers (figure S4). (b) Built-in electric field at the interface to effectively transfer photo-generated carriers. (c) Epitaxial nature of 2D Bi layer with less defects to allow efficient charge transport.

Moreover, we investigate key optoelectronic parameters for 2D Bi/Si(111) heterojunction. Responsivity (R_{ph}) is an important parameter that reflects the sensitivity to the incident light as defined by $R_{ph} = I_{ph}/P_I$, where I_{ph} is the photocurrent and P_I is the incident light power. The power-dependent responsivity of 2D Bi/Si(111) and control group Si devices are plotted in semi-logarithmic scale (figure 4(a)). The photoresponsivity tends to decrease with an improvement of light intensity, which can be attributed to the increase of carrier recombination [20]. Notably, photoresponsivity of ~80 A W^{-1} under 0.1 μW outperforms the nanostructure silicon photodetectors [21]. Based on above results of responsivity, detectivity (D^*) and external quantum efficiency (EQE) are depicted in figure 4(b). D^* evaluates the capability of a photodetector to detect weak light quantitatively. Assuming that the dark current is dominated by shot noise which is independent of frequency [22], D^* can be calculated via the following formula [23]:

$$D^* = \frac{A^{1/2} R_{ph}}{(I_{dark} 2q)^{1/2}}. \quad (1)$$

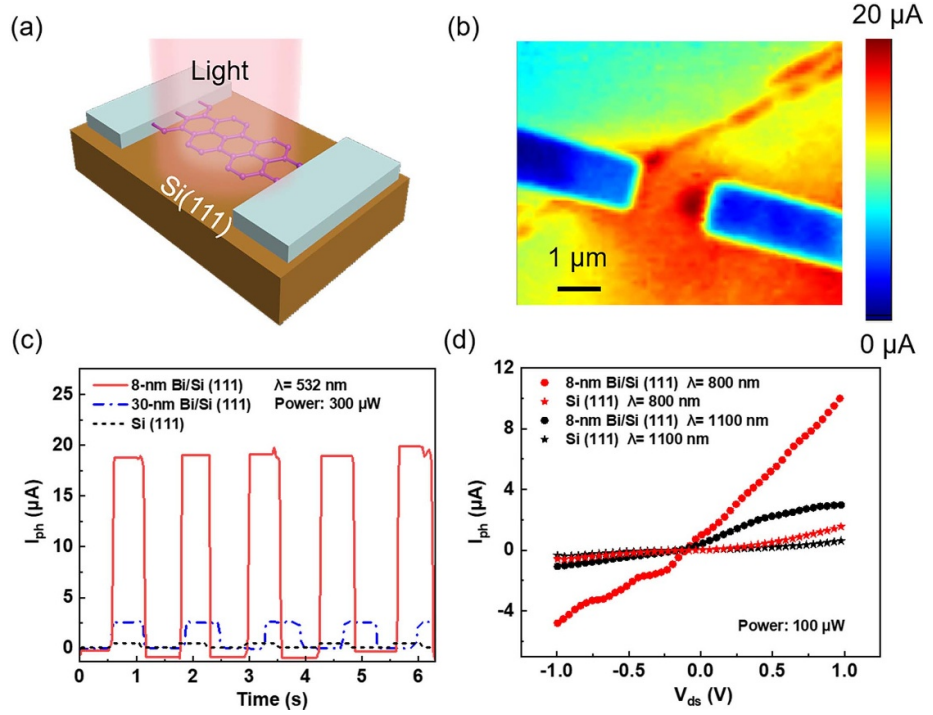

Figure 3. Photocurrent generation in 2D Bi/Si(111) optoelectronic devices. (a) Schematics of the device layout. (b) Scanning photocurrent image under 520 nm laser exposure at 300 μW. Photocurrent generation under (c) 532 nm laser exposure at 300 μW and (d) 800 nm and 1100 nm laser at 100 μW.

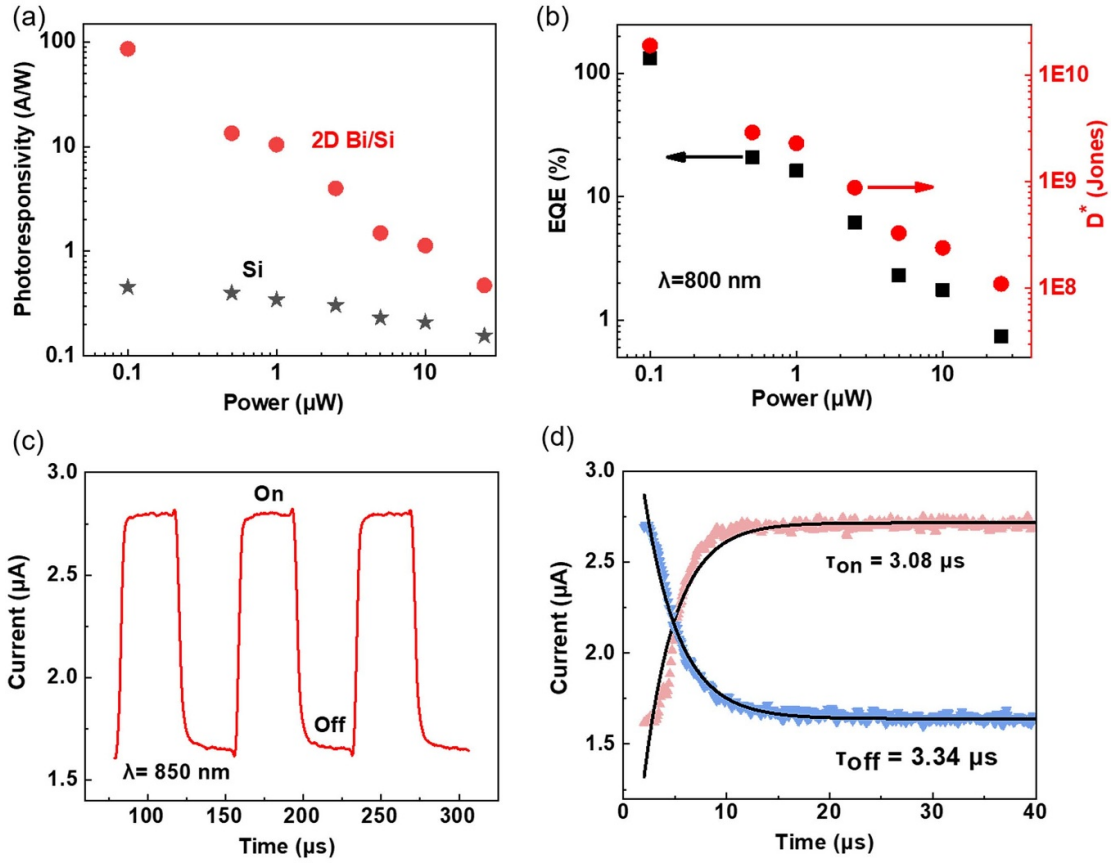

Figure 4. Optoelectronic performance of 2D Bi/Si(111) devices. (a) Extracted power dependence photoresponsivity for bare Si(111) and 2D Bi/Si(111) at 1 V bias under ambient environment. (b) Detectivity (D^*) and external quantum efficiency (EQE) as a function of laser power under 800 nm illumination. (c) Photoresponse of a 2D Bi/Si(111) detector to pulsed 850 nm light irradiation with a frequency of 10 kHz. (d) Enlarged response time curve of 2D Bi/Si(111) heterojunction under 850 nm illumination. The τ_{on} and τ_{off} are 3.08 μs and 3.34 μs respectively.

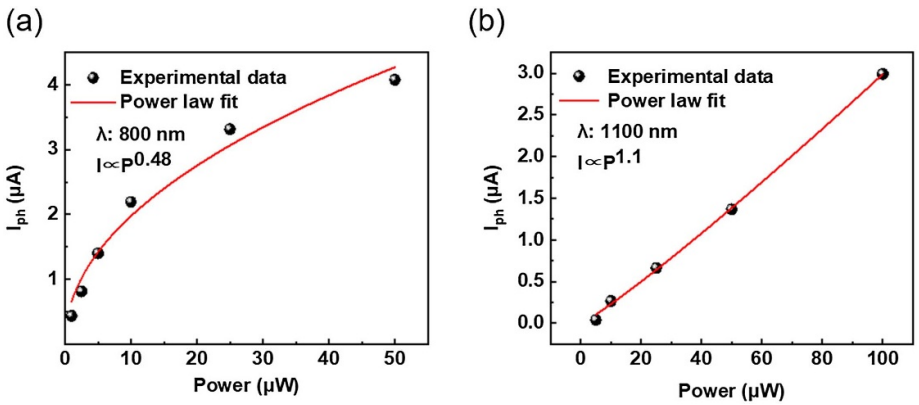

Figure 5. Relationship between the photocurrent and light intensity. 8 nm Bi/Si heterojunction's photocurrent output at 1 V bias as a function of light intensity with (a) 800 nm and (b) 1100 nm laser illumination. The power law fitting indicates the relationship of photocurrent with light intensity and the factor θ reveals the role of trap states.

where A represents the detector area, R_{ph} is photo responsivity as mentioned above and I_{dark} is the dark current. Under 800 nm illumination, D^* increases when the laser power diminishes as shown in figure 4(b) and reaches 1.9×10^{10} Jones (cm $Hz^{1/2}$ W^{-1}). The relatively small detectivity can be attributed to dark current $\sim\mu$A [24, 25]. EQE exhibits the population ratio of collected charge carriers (N_C) to incident photons N_I, which can be expressed as following [26]:

$$\mathrm{EQE} = \frac{N_C}{N_I} = R_{ph}\frac{hc}{q\lambda}. \quad (2)$$

where h is the Planck constant, c is the speed of light, q and λ refer to electron charge and wavelength of incident light respectively. EQE (%) of our 2D Bi/Si(111) heterojunction reaches its maximum up to 140 (%) at the power of 0.1 μW (left axis of figure 4(b)). Over 100 (%) EQE value results from photo gain associated with trap states [27] that will be discuss later.

For the practical use of a photodetector, response time is a key parameter. Figure 4(c) shows the time response when 850 nm light is switched on or off by an acoustic optical modulator at a frequency of 10 kHz (figure 4(c)). The response behavior can be well retained after several repeats. The magnified and detailed response time (figure 4(d)) includes rise and decay two components [28]. Dynamic characteristics of our devices in response to illumination could be well described by $I(t) = I_0 + A\exp(-t/\tau)$, where τ is a constant indicating the lifetime of carriers, I_0 is the dark current, and A is a coefficient. According to the fitting curve, rise (τ_{on}) and decay (τ_{off}) time of our 2D Bi/Si(111) can be calculated as $\sim$3.08 and $\sim$3.34 μs respectively.

We further investigate the role of trap states that related with photo gain effect [29]. Response performance under varied laser powers is displayed in figure 5. Interestingly, photocurrent and light intensity fits in a power law $I_{ph} = P_I{}^{\theta}$ relation, where P_I represents power of incident light and θ can be regarded as a result of trapping and recombination of photoinduced carriers [30]. The fitting curve shows that θ equals to 0.48 under 800 nm illumination (figure 5(a)) while increasing to 1.1 under 1100 nm wavelength (figure 5(b)). We believe that under 800 nm illumination, photo generated carriers interact with trap states at Si interface [31], thus leading to a photo gain with $\theta < 1$. Nevertheless, under 1100 nm illumination, carriers mainly transport through the surface of MBE 2D Bi with less impact of defect-induced trap states [12] accompanying with $\theta > 1$.

The mechanism for photocurrent generation in our 2D Bi/Si(111) is depicted in figure 6. As 2D Bi and Si form into type-I heterojunction according to band gap of 2D Bi (figure S5), electrons tend to transfer towards Bi layer (path I) if not trapped at Si interface. After entering conductive 2D Bi, photogenerated carriers transport and be collected to electrodes under bias voltage (path II). Part of photogenerated electrons recombine with holes during the process (path III). By tuning thickness and other parameters, it is desired to promote step I and II while limiting step III for a better photocurrent effect [7].

Table 2 summarizes several key parameters about reported Bi-related materials [32, 33], and it shows that 2D Bi/Si(111) heterojunction in this work outperformed standalone Bi thin film or silicon photodetectors. Moreover, the heterojunction device has achieved unprecedented performance in terms of high responsivity and response speed compared with typical Bi_2 (Te, Se)$_3$ photodetectors [34] while maintaining a decent air-stability (figures S6 and S7). Inspiringly, our first attempt of combining 2D Bi with Si(111) as a heterojunction device reveals that the heterojunction can achieve high responsivity and short response time simultaneously. Similar coupling effect

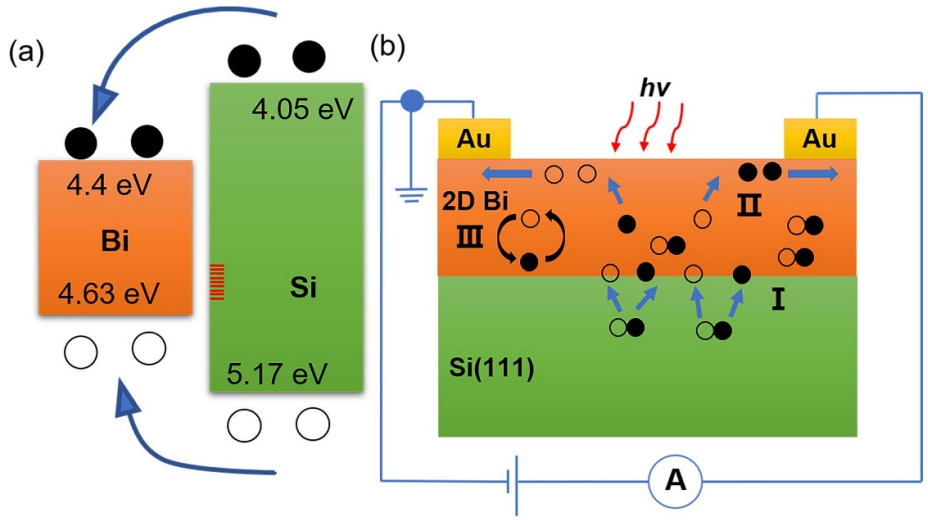

Figure 6. Working mechanism of 2D Bi/Si heterojunction optoelectronic devices. (a) Schematic band-alignment diagram of Bi/Si junction (drawing not in scale for visualization purpose) with short red lines denoting the location of trap states. (b) Mechanism of photo current generation in 2D Bi/Si heterojunction with black dots and circles referring to electrons and holes respectively.

Table 2. Performance of Bi based photodetector.

Materials	Wavelength (nm)	R (A W^{-1})	τ_{rise} (ms)	Note
Bi_2Te_3/Si	635	1	100	[36]
Bi_2Te_3/Graphene	980	10	8.7	[37]
Bi_2Se_3	808	24.28	0.0025	[38]
Bi thin film (200 nm)	635	0.25	900	[7]
Porous silicon	1000	0.6	/	[39]
2D Bi/Si(111)	800	80	0.003	This work

has also been found in some metal oxide material systems [35].

In summary, we investigate the electronic characteristics and photoresponse of 2D Bi grown on Si(111) substrates. The 2D Bi/Si(111) heterojunction possesses a high responsivity up to 80 A W^{-1} and a rapid response around 3 μs, which are several orders of magnitude higher than Bi-alone thin film. Such improved performance is due to combined light absorption, efficient carries transfer with built-in field in epitaxial 2D Bi on Si(111). Our work reveals that 2D Bi/Si(111) heterojunction is feasible to develop high-performance photodetectors and offers a new strategy to integrate other group VA Xenes in optoelectronic devices.

3. Methods

3.1. Material characterization

As-prepared samples are characterized by scanning electron microscope (FEI Sirion) and AFM (Asylum Research MFP-3D-SA) to confirm morphology and thickness of 2D Bi. EDXs (FEI Sirion) is performed to verify elemental composition. The crystallinity of 2D Bi is characterized by XRD (Smart Lab Cu Kα). Raman measurements (Horiba JY HR800) are carried out under the wavelength of 532 nm laser with 50× objective lens and a numerical aperture of 0.5.

3.2. Device fabrication

Metal electrodes are patterned via electron beam lithography (FEI, FP2031/12 INSPECT F50) followed by 5 nm Ti/50 nm Au deposition via electron-beam evaporation (VNANO VZS-600Pro) and then a lift-off process. Electrical transport measurements are conducted with a semiconductor analyzer (Keithley 2612) under ambient conditions. Carrier mobility is derived from Hall effect test system (HET-RT) under 600 mT magnetic field at 290 K.

3.3. Photodetector characterization

The photoresponse characteristics of NIR are measured using a He–Ne laser (CNI MRL-III-633) and Chameleon with Compact OPO (Coherent Inc.) A digital storage oscilloscope (Tektronix TDS 1012) is used to measure the transient response of the photocurrent. The laser beam is focused on the sample with a 50× objective lens to obtain a spot size of ~2 μm. Photocurrent mapping derives from a photocurrent scanning test microscope system (Meta Corporation MStarter 200). All the optoelectronic characterization measurements are implemented at room temperature under ambient conditions.

Data availability

The data that support the findings of this study are available upon reasonable request from the authors.

Acknowledgments

We thank Beibei Zhu and Yamei Ding for manuscript revision. L T acknowledges the support from National Natural Science Foundation of China (51602051), Jiangsu Province Innovation Talent Program and Jiangsu Province Six-Category Talent Program (DZXX-011). Z N acknowledges the support from National Natural Science Foundation of China (61927808) and Strategic Priority Research Program of Chinese Academy of Sciences (XDB30000000).

Author contributions

L T and Z H N conceived and directed the project. E S W prepared the 2D Bi samples under guidance from S R B, Z Y D and W H W designed and fabricated devices. Z Y D, W H W and J Y C performed the measurements and analyzed the experimental data. L T, Z H N, W H W and Z Y D contributed to the writing. All authors contributed to discussions on the manuscript.

Conflict of interest

The authors declare no competing interests.

ORCID iDs

Zhenhua Ni https://orcid.org/0000-0002-6316-2256
Li Tao https://orcid.org/0000-0001-6055-6068

References

[1] Li C, Cao Q, Wang F, Xiao Y, Li Y, Delaunay J J and Zhu H 2018 Engineering graphene and TMDs based van der Waals heterostructures for photovoltaic and photoelectrochemical solar energy conversion *Chem. Soc. Rev.* **47** 4981–5037
[2] Zhang Z, Lin P, Liao Q, Kang Z, Si H and Zhang Y 2019 Graphene-based mixed-dimensional van der Waals heterostructures for advanced optoelectronics *Adv. Mater.* **31** 1806411
[3] Rao G *et al* 2019 Two-dimensional heterostructure promoted infrared photodetection devices *InfoMat* **1** 272–88
[4] Lu Y *et al* 2015 Topological properties determined by atomic buckling in self-assembled ultrathin Bi(110) *Nano Lett.* **15** 80–87
[5] Ning W, Kong F Y, Han Y Y, Du H F, Yang J Y, Tian M L and Zhang Y H 2014 Robust surface state transport in thin bismuth nanoribbons *Sci. Rep.* **4** 7086
[6] Zhang S, Xie M, Li F, Yan Z, Li Y, Kan E, Liu W, Chen Z and Zeng H 2016 Semiconducting group 15 monolayers: a broad range of band gaps and high carrier mobilities *Angew. Chem., Int. Ed. Engl.* **55** 1666–9
[7] Yao J D, Shao J M and Yang G W 2015 Ultra-broadband and high-responsive photodetectors based on bismuth film at room temperature *Sci. Rep.* **5** 12320
[8] Huang H *et al* 2018 Two-dimensional bismuth nanosheets as prospective photo-detector with tunable optoelectronic performance *Nanotechnology* **29** 235201
[9] Zhou Q Q L, Lu D and Tang H 2020 Self-powered ultra-broadband and flexible photodetectors based on the bismuth films by vapor deposition *ACS Appl. Electron. Mater.* **2** 1254–62
[10] Yao J, Zheng Z, Shao J and Yang G 2015 Promoting photosensitivity and detectivity of the Bi/Si heterojunction photodetector by inserting a WS_2 layer *ACS Appl. Mater. Interfaces* **7** 26701–8
[11] Nagao T, Doi T, Sekiguchi T and Hasegawa S 2000 Epitaxial growth of single-crystal ultrathin films of bismuth on Si(111) *J. Phys. D: Appl. Phys.* **39** 4567–70
[12] Walker E S *et al* 2016 Large-area dry transfer of single-crystalline epitaxial bismuth thin films *Nano Lett.* **16** 6931–8
[13] Lu D L, Luo S W, Liu S H, Yao H, Ren X H, Zhou W C, Tang D S, Qi X and Zhong J X 2018 Anomalous temperature-dependent Raman scattering of vapor-deposited two-dimensional Bi thin films *J. Phys. Chem.* C **122** 24459–66
[14] Kumari L, Lin J H and Ma Y R 2008 Laser oxidation and wide-band photoluminescence of thermal evaporated bismuth thin films *J. Phys. D: Appl. Phys.* **41** 7
[15] Haro-Poniatowski E, Jouanne M, Morhange J F, Kanehisa M, Serna R and Afonso C N 1999 Size effects investigated by Raman spectroscopy in Bi nanocrystals *Phys. Rev.* B **60** 10080–5
[16] Xiao S, Wei D and Jin X 2012 Bi(111) thin film with insulating interior but metallic surfaces *Phys. Rev. Lett.* **109** 166805
[17] Sun X, Zhao H, Chen J, Zhong W, Zhu B and Tao L 2021 Effects of the thickness and laser irradiation on the electrical properties of e-beam evaporated 2D bismuth *Nanoscale* **13** 2648–57
[18] Yang Z, Wu Z, Lyu Y and Hao J 2019 Centimeter-scale growth of two-dimensional layered high-mobility bismuth films by pulsed laser deposition *InfoMat* **1** 98–107
[19] Wu J, Chen Y, Wu J and Hippalgaonkar K 2018 Perspectives on thermoelectricity in layered and 2D materials *Adv. Electron. Mater.* **4** 1800248
[20] Jiang J *et al* 2018 Defect engineering for modulating the trap states in 2D photoconductors *Adv. Mater.* **30** 1804332
[21] Mulazimoglu E, Coskun S, Gunoven M, Butun B, Ozbay E, Turan R and Unalan H E 2013 Silicon nanowire network metal-semiconductor-metal photodetectors *Appl. Phys. Lett.* **103** 083114
[22] Wang F, Li L, Huang W, Li L, Jin B, Li H and Zhai T 2018 Submillimeter 2D Bi_2Se_3 flakes toward high-performance infrared photodetection at optical communication wavelength *Adv. Funct. Mater.* **28** 1802707
[23] Lv P, Zhang X J, Zhang X W, Deng W and Jie J S 2013 High-sensitivity and fast-response graphene/crystalline silicon Schottky junction-based near-IR photodetectors *IEEE Electron Device Lett.* **34** 1337–9
[24] Zhou X, Gan L, Tian W, Zhang Q, Jin S, Li H, Bando Y, Golberg D and Zhai T 2015 Ultrathin $SnSe_2$ flakes grown by chemical vapor deposition for high-performance photodetectors *Adv. Mater.* **27** 8035–41
[25] Wang L, Jie J, Shao Z, Zhang Q, Zhang X, Wang Y, Sun Z and Lee S-T 2015 MoS_2/Si heterojunction with vertically standing layered structure for ultrafast, high-detectivity, self-driven visible-near infrared photodetectors *Adv. Funct. Mater.* **25** 2910–9
[26] Chitara B, Panchakarla L, Krupanidhi S and Rao C 2011 Infrared photodetectors based on reduced graphene oxide and graphene nanoribbons *Adv. Mater.* **23** 5419–24
[27] Tan H, Fan Y, Zhou Y, Chen Q, Xu W and Warner J H 2016 Ultrathin 2D photodetectors utilizing chemical vapor deposition grown WS_2 with graphene electrodes *ACS Nano* **10** 7866–73

[28] Tang W, Politano A, Guo C, Guo W, Liu C, Wang L, Chen X and Lu W 2018 Ultrasensitive room-temperature terahertz direct detection based on a bismuth selenide topological insulator *Adv. Funct. Mater.* **28** 1801786
[29] Luo P, Zhuge F W, Wang F K, Lian L Y, Liu K L, Zhang J B and Zhai T Y 2019 PbSe quantum dots sensitized high-mobility Bi_2O_2Se nanosheets for high-performance and broadband photodetection beyond 2 μm *ACS Nano* **13** 9028–37
[30] Zhang W J, Huang J K, Chen C H, Chang Y H, Cheng Y J and Li L J 2013 High-gain phototransistors based on a CVD MoS_2 monolayer *Adv. Mater.* **25** 3456–61
[31] Tan C S, Zhao Y, Guo R H, Chuang W T, Chen L J and Huang M H 2020 Facet-dependent surface trap states and carrier lifetimes of silicon *Nano Lett.* **20** 1952–8
[32] Zhang X, Wang J and Zhang S-C 2010 Topological insulators for high-performance terahertz to infrared applications *Phys. Rev.* B **82** 245107
[33] Zheng W *et al* 2015 Patterning two-dimensional chalcogenide crystals of Bi_2Se_3 and In_2Se_3 and efficient photodetectors *Nat. Commun.* **6** 6972
[34] He H-T, Wang G, Zhang T, Sou I-K, Wong G K L, Wang J-N, Lu H-Z, Shen S-Q and Zhang F-C 2011 Impurity effect on weak antilocalization in the topological insulator Bi_2Te_3 *Phys. Rev. Lett.* **106** 166805
[35] Sarcan F, Orchard S, Kuerbanjiang B, Skeparovski A, Lazarov V K and Erol A 2020 Ultraviolet photodetector based on $Mg_{0.67}Ni_{0.33}O$ thin film on $SrTiO_3$ *Phys. Status Solidi* **14** 2000175
[36] Yao J D, Shao J M, Wang Y X, Zhao Z R and Yang G W 2015 Ultra-broadband and high response of the Bi_2Te_3–Si heterojunction and its application as a photodetector at room temperature in harsh working environments *Nanoscale* **7** 12535–41
[37] Qiao H *et al* 2015 Broadband photodetectors based on graphene-Bi_2Te_3 heterostructure *ACS Nano* **9** 1886–94
[38] Zhang H, Zhang X, Liu C, Lee S-T and Jie J 2016 High-responsivity, high-detectivity, ultrafast topological insulator Bi_2Se_3/silicon heterostructure broadband photodetectors *ACS Nano* **10** 5113–22
[39] Lee M K, Chu C H, Wang Y H and Sze S M 2001 1.55 μm and infrared-band photoresponsivity of a Schottky barrier porous silicon photodetector *Opt. Lett.* **26** 160–2